processes

MDPI

Article

Performance Analysis of Effective Methylene Blue Immobilization by Carbon Microspheres Obtained from Hydrothermally Processed Fructose

Sanja S. Krstić [1], Đuro Čokeša [1], Radojka T. Vujasin [1], Branka V. Kaluđerović [1], Milan Z. Momčilović [2,*], Darko Jaćimovski [3], Pavel Gurikov [4,5] and Vladimir M. Dodevski [1,*]

[1] Laboratory of Materials, Vinča Institute of Nuclear Sciences–National Institute of the Republic of Serbia, University of Belgrade, 11351 Belgrade, Serbia; ssanjak@vinca.rs (S.S.K.); cokesadj@vinca.rs (Đ.Č.); radojka.vujasin@vin.bg.ac.rs (R.T.V.); branka@vinca.rs (B.V.K.)
[2] Department of Chemistry, Faculty of Sciences and Mathematics, University of Niš, Višegradska 33, 18000 Niš, Serbia
[3] Institute of Chemistry, Technology and Metallurgy, National Institute of the Republic of Serbia, University of Belgrade, 11000 Belgrade, Serbia; darko.jacimovski@ihtm.bg.ac.rs
[4] Institute of Thermal Separation Processes, Hamburg University of Technology, Eißendorfer Str. 38, 21073 Hamburg, Germany; pavel.gurikov@tuhh.de
[5] Aerogel-it GmbH, Albert-Einstein-Str. 1, 49076 Osnabrück, Germany
* Correspondence: milanmomcilovic@yahoo.com (M.Z.M.); vladimir@vin.bg.ac (V.M.D.)

Abstract: Carbon microspheres have been synthesized by the hydrothermal method with fructose and a phosphoric acid solution at two different concentrations, which were used as precursors. The obtained materials were characterized by elemental analysis, X-ray powder diffraction (XRPD) analysis, scanning electron microscopy (SEM), nitrogen adsorption/desorption measurements, and Fourier transform infrared (FTIR) spectroscopy. Batch sorption experiments were performed to remove methylene blue (MB) from aqueous solutions by varying the initial concentration of MB (C_0) from 50 to 500 mg/dm^3, contact period, solution pH value, and temperature. Prepared sorbents consisted of microsphere particles with diameters in the range of 0.6–2.7 µm. The synthetic route was found to govern the microporous–mesoporous structure and surface acidic functional groups of the final product. A phosphoric acid concentration of 40 wt.% gave carbon material with a specific surface area of 932 m^2/g and a total pore volume of 0.43 cm^3/g. It was found that the extent of MB sorption by the obtained carbon microspheres increased with initial dye concentration, contact time, and especially solution pH but slightly decreased with increasing temperature. Kinetic studies showed that the dye sorption process followed pseudo-second-order kinetics.

Keywords: hydrothermal synthesis; carbonization; fructose; methylene blue; removal

Citation: Krstić, S.S.; Čokeša, Đ.; Vujasin, R.T.; Kaluđerović, B.V.; Momčilović, M.Z.; Jaćimovski, D.; Gurikov, P.; Dodevski, V.M. Performance Analysis of Effective Methylene Blue Immobilization by Carbon Microspheres Obtained from Hydrothermally Processed Fructose. *Processes* **2024**, *12*, 2683. https://doi.org/10.3390/pr12122683

Academic Editor: Anna Wołowicz

Received: 3 November 2024
Revised: 21 November 2024
Accepted: 26 November 2024
Published: 28 November 2024

1. Introduction

Size-controlled activated carbon materials with their large sorption capabilities and high porosity have been widely investigated in advanced material science. Increasing environmental problems also increase the need for novel materials with a large variety of applications, primarily as sorbents and filter materials [1,2], catalysts [3,4], supercapacitors [5], energy storage and conversion systems [6], drug delivery mechanisms [7], separation technologies [8], Li-ion battery anodes [9], etc. Spherical activated carbons are receiving growing attention due to their diverse potential in many applications, in contrast to granular or powdered carbon materials, and their desirable characteristics such as high wear resistance and mechanical properties, good sorption capacity, very good purity, smooth surface and uniformity of particle size and shape, good fluidity, excellent packaging possibility, low pressure drop, high bulk density and micropore volume, low ash and impurity content, and controllable pore size distribution [10].

Activated carbons are usually prepared by pyrolysis and activation of organic starting materials. The activation process may be conducted by physical and chemical methods. Both methods can generate carbons with large specific surface areas, which is crucial for their large sorption capacities [11,12]. Unfortunately, both pyrolysis and activation methods have many disadvantages, such as high energy costs, low carbon yield, and waste gas emissions. Numerous investigations at the global level have been conducted in the last two decades in the field of conversion of carbohydrates to carbon-based materials by one-step methods and without using catalysts [13,14]. Regarding the preparation of spherical carbons, the method used for the synthesis process strongly depends on the selected precursor. In the case of polymeric starting materials, polymerization reactions are used for the preparation of spherical carbons [15]. For carbohydrates, hydrothermal treatment has been one of the best methods in recent years considering mild synthesis conditions [16–18]. There are lots of advantages to using different types of sugar as a carbon precursor, such as low cost, availability, high purity, and the existence of aromatic rings that are necessary for forming graphitic carbon structures in the obtained material. The carbon materials obtained using sugars have been found to possess spherical morphology in general, great thermal stability, and good electrical conductivity [19,20]. However, the carbon materials obtained by the hydrothermal carbonization of sugars have limited surface area and low porosity. This property directly affects their eventual applications. In order to resolve this shortcoming, it has been proposed to include additional post-treatment after the hydrothermal heating by pyrolysis or activation step at higher temperatures (>600 °C), which would result in increased porosity within the structure of the material [21,22]. The pore organization of the activated carbon material could be controlled by different methods, such as activation conditions (activation agent, temperature, and time), type of precursor, or modification after synthesis. The most commonly used chemical activation agents are NaOH, KOH, and H_3PO_4 [23–26].

Sorption of organic waste from the aqueous phase is one of the most important applications of carbon-based materials [27]. Environmental pollution caused by textile industry wastewater has received widespread attention and interest globally in the last two decades [28,29]. Dyes discharged from the food, leather, textile, and other industries are the main organic pollutants in natural water. A large number of organic dyes are environmentally toxic, carcinogenic and mutagenic, mostly non-biodegradable, and cause severe health damage to humans, animals, plants, and microorganisms [30–32].

Wastewater from the textile and leather industries contains high amounts of azo dyes such as MB, methyl orange, and Congo red. MB is a cationic dye mostly used for dying cotton, wood, and silk [29].

In this work, carbon microspheres were obtained by the hydrolysis of fructose with phosphoric acid through facile and inexpensive hydrothermal carbonization. This method of synthesis generates carbon-based materials with a high concentration of surface oxygen functional groups such as carboxyl, carbonyl, lactones, phenols, etc. [33,34]. The sorption of dyes and pigments onto different activated carbons has been widely investigated [35–37] and it has shown high efficiency and very good results.

The main objective of this work is to examine the possibility of fructose as a low-cost precursor for the preparation of carbonaceous material with high surface area and to apply it for MB sorption from an aqueous solution. For this purpose, carbon microspheres were synthesized with two different concentrations of phosphoric acid, resulting in dissimilar textural properties. They were properly characterized and examined in a batch system for the removal of MB from the aqueous phase under varying experimental conditions, including initial dye concentrations, pH, contact time, and temperature. In this way, a well-studied compound was used as a benchmark sorbate for evaluating the sorptive potential of the obtained carbon microspheres. Finally, the whole study is directed towards the purification of wastewaters from the textile industry by means of hydrothermally derived carbons as a concept for their prospective utilization.

2. Materials and Methods

2.1. Chemical and Reagents

Orthophosphoric acid was purchased from Merck KGaA (Darmstadt, Germany) (85%, 1.71 g/cm^3). Methylene blue was also supplied by Merck KGaA (Darmstadt, Germany) (purity: for the staining of blood constituents, as declared) was dried for 2 h at 90 °C prior to use. D (-)-Fructose ≥95% ($C_6H_{12}O_6$, Mr = 180.16 g/mol, ρ = 1.59 g/cm^3, melting point 105 °C) was obtained from Carl ROTH (Karlsruhe, Germany). Deionized water with a resistivity of 18 MΩ/cm was used to prepare all solutions. All chemicals employed were used without purification.

2.2. Sample Preparation

Hydrothermal synthesis of carbon microspheres was performed in a glass reactor by using 40% and 80% (wt.%) H_3PO_4 as an activating agent. Fructose solution of 2M concentration was homogenized by magnetic stirrer for a period of 15 min, poured in a glass reactor, and then placed into the dry oven at 250 °C under autogenously formed pressure for 20 h. Prepared samples were washed with distilled water in an ultrasonic bath at 60 °C. The next step was filtration and washing with distilled water to neutral. Finally, the samples were dried in an oven at 100 °C and labeled as AC40 and AC80, depending on the concentration of H_3PO_4 used in the experiment (40% or 80%, respectively).

2.3. Characterization

Elemental analyses of the synthesized carbon microsphere materials were investigated on a Vario EL III C, H, N, S/O Elemental Analyzer. The amounts of C, N, and H were determined directly, while the amount of oxygen was calculated as 100%–C%–N%–H%. The absence of S is implied.

The crystal structure of the synthesized samples was characterized using X-ray powder diffraction (XRPD) analysis using an Ultima IV Rigaku diffractometer with a Cu Kα 1,2 radiation source. Samples were recorded in the range of 10–90° 2θ, with a scanning step size of 0.02° and at a scan rate of 2°/min. The interlayer distance (d_{002}) and crystallite height (L_c) were determined from the (002) diffraction peak, and crystallite width and size (L_a), along the basal plane, from the θ position of the diffraction peak (100). The calculations were performed with the Bragg and Scherrer formulas.

The morphology of carbon samples obtained in this work was characterized by SEM—JEOL JSM–5800. The sphere diameter range was determined by applying the Image Pro Design program and the results were presented in the form of histograms.

The FTIR spectra of the as-prepared carbon microspheres, before and after the sorption of the methylene blue, were recorded using the Perkin Elmer Spectrum Two FT-IR spectrometer. The diffuse reflectance infrared Fourier transform (DRIFT) technique was used for collecting the spectra.

Textural characteristics of carbon microspheres were determined by measuring nitrogen adsorption/desorption isotherms at 77 K by the gravimetric McBain balance method. The values of specific surface area (S_{BET}) were calculated from adsorption data applying the standard Brunauer–Emmet–Teller (BET) method [38,39]. The best linear fit that was used for calculation was in the region $p/p_0 < 0.05$ (p and p_0 represent the equilibrium and saturation pressures). The total pore volume V_{tot} was measured at the relative pressure $p/p_0 = 0.96$, applying Gurvitch's rule [38]. The Dubinin–Radushkevich (D-R) equation was used for calculation of micropore volume (VDR) and characteristic adsorption energy (E_0) [40].

The effective micropore size (L) distribution was calculated according to the Horvath and Kawazoe (HK) method [41]. The most commonly applied Barrett, Joyner, and Halenda (BJH) method for mesopore-containing materials [42] was used to determine the pore size (w) distribution for pores higher than 1.4 nm. Both methods were applied to the appropriate part of the desorption branch of the N_2 isotherm.

By using the high-resolution α_s–plot method [43,44], the total surface area (S_{TOT}), external surface area (S_{EXT}), and micropore volume ($V_{mic\alpha}$) were estimated. Micropore surface area (S_{mic}) was calculated by subtracting S_{EXT} from the S_{TOT} [44].

2.4. Sorption Experiments

Batch MB sorption experiments were carried out to investigate the effects of contact time, initial dye concentration, pH, and temperature on the sorption of MB onto two synthesized samples of carbon microspheres by varying the parameters under study while keeping the other parameters constant.

Examination of the MB sorption kinetics on the synthesized materials was performed by monitoring the change in the concentration of MB (C_t) over time (t). During the MB sorption from aqueous solutions for initial concentrations (C_0) of 50, 100, 150, 200, 300, 400, and 500 mg/dm^3, each concentration was adjusted to two pH values (7 and 12) with 0.1 M NaOH and 0.1 M HCl. Before that, both samples were tested at three pH values: 5, 7, and 12, for the probes with an initial MB concentration of 300 mg/dm^3. Sorption equilibrium was established by intensive mixing of the given mixture, made of 50 mg of the carbon sample and 50 cm^3 of MB solution by magnet stirring at a temperature of 25 °C. For testing the process kinetics, at certain time intervals, stirring was stopped and the sample was centrifuged for 1 min. After that, a sample of the liquid phase with a volume of 1 cm^3 was taken, and stirring was continued. The sample was diluted 100 times, and the concentration was measured for a given time on a UV-VIS spectrophotometer, Thermo Fisher Scientific (Waltham, MA, USA) Evolution 60 S, at a wavelength of 665 nm.

The amounts of the sorbed MB per unit mass of synthesized carbon microspheres (sorption capacities) were calculated by taking into account the differences between the initial and final MB concentrations in solution using the following equation:

$$q_t = \frac{(C_0 - C_t)V}{m} \quad (1)$$

where q_t (mg/g) is the sorption capacity of MB at any time t (min), C_0 and C_t (mg/dm^3) are MB initial concentration and concentration at any time t, V (dm^3) is the volume of the MB solution, and m (g) is the mass of the sorbent used in the experiments.

3. Results and Discussion

3.1. Elemental Analysis

The content of elements C, H, and O in the carbon microsphere samples obtained after hydrothermal treatment of fructose with H_3PO_4 was determined by elemental analysis. The results are listed in Table 1 and graphically presented in Figure 1. The amounts of C and H were determined directly, while the amount of oxygen was calculated as 100%–C%–H%.

Table 1. Elemental analysis and yields of the obtained carbon samples.

Sample	C (%)	H (%)	O (%)
Fructose	40	7	53
AC80	72	9	19
AC40	76	5	19

The presented results show that the content of carbon in the sample synthesized with 40% H_3PO_4 was slightly higher (by 4%) compared to the sample obtained with 80% H_3PO_4. That is followed by a decrease in hydrogen content in sample AC 80.

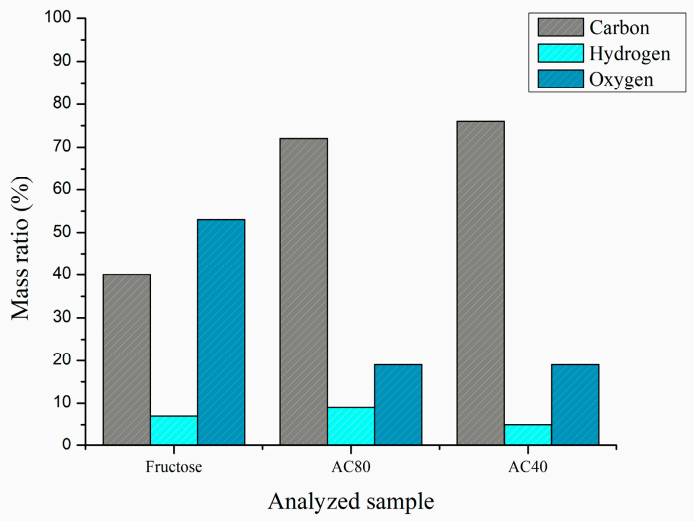

Figure 1. Elemental analysis and yields of the obtained carbon samples.

3.2. XRD

The XRPD patterns of the AC80 and AC40 samples, presented in Figure 2, showed form characteristics for amorphous carbonaceous materials.

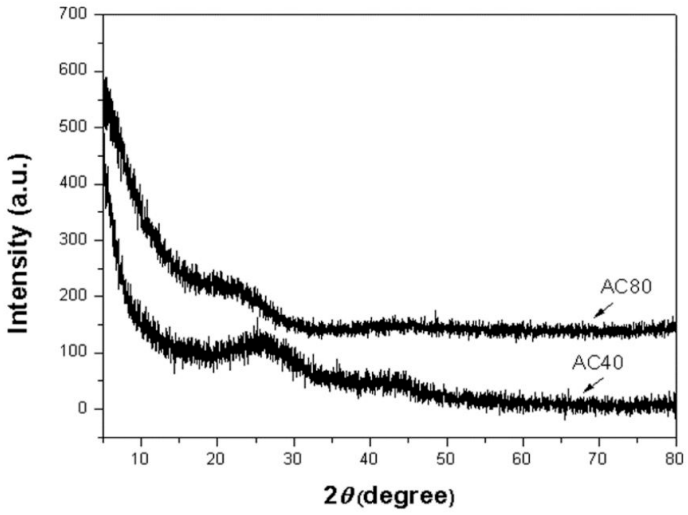

Figure 2. The XRPD patterns of the synthesized carbon microspheres.

For sample AC40, two broad peaks are observed near 2θ 26 and 42°, which are attributed to reflections (002) and (100), respectively. These features are attributed to the carbons-based materials. The value for interlayer distance d_{002} is 0.376 nm, the crystallite height L_c is 1.082 nm, and the value for the crystallite width L_a is 1.961 nm. Therefore, these materials have a turbostratic structure with small crystallites with domain sizes in the range of 1–2 nm.

3.3. Scanning Electron Microscopy

The morphology of the samples is presented by the SEM micrographs in Figure 3a,b. The obtained carbon materials consist of particles with a spherical morphology as shown by the SEM micrographs. It is visually noticeable that the microspheres of the sample obtained with a more concentrated solution of phosphoric acid (AC80) are significantly smaller in diameter than the sample made with 40% phosphoric acid.

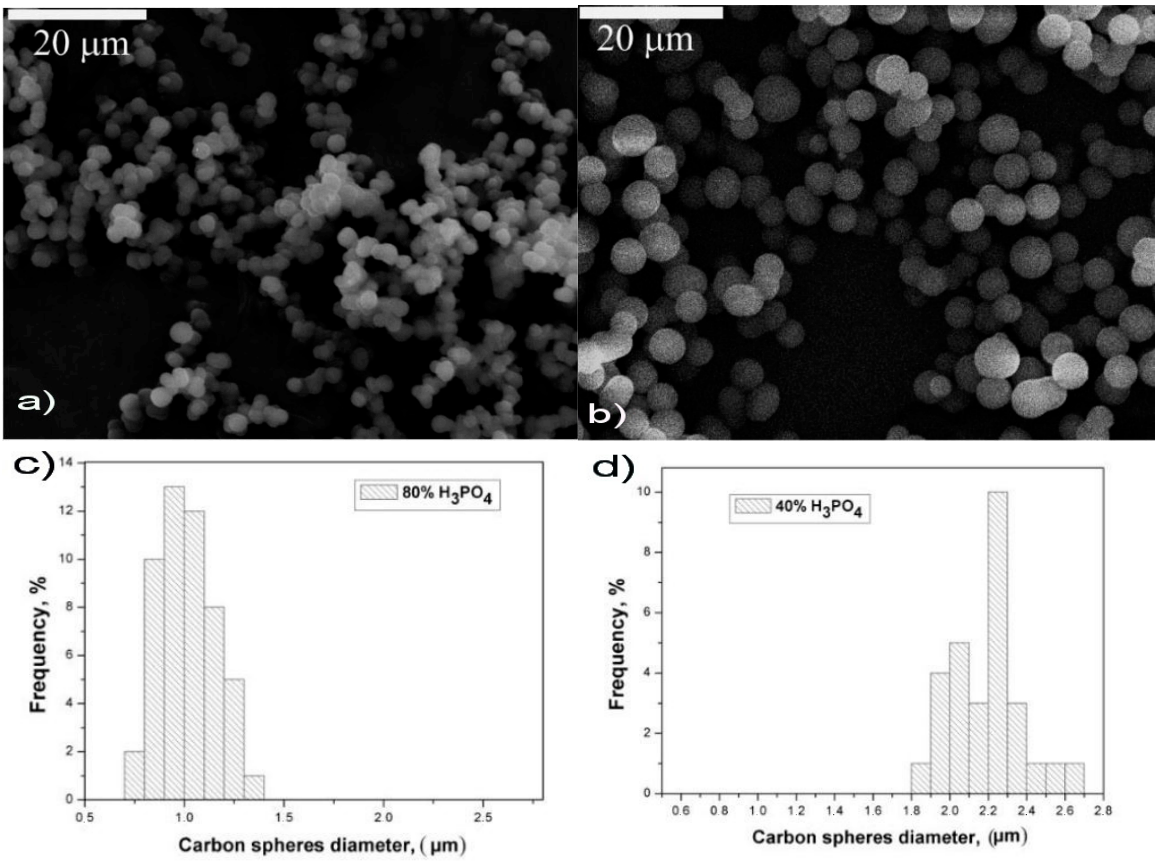

Figure 3. SEM micrographs of (**a**) AC80 and (**b**) AC40, and calculated diameter of (**c**) AC80 and (**d**) AC40 carbon microspheres.

The microsphere diameter range was determined by applying the Image Pro Design program, and the results were presented in the form of histograms in Figure 3c,d. The diameter of the obtained particles of the AC80 sample is in the range of 0.75 to 1.37 mm. The most common are microparticles with a diameter of 1 μm (see Figure 3c). The particle diameter of the sample obtained with less concentrated phosphoric acid (AC40) is larger and ranges from 1.8 to 2.7 μm, with the most pronounced diameter of 2.3 μm (see Figure 3d). It may be seen from the micrographs that the diameter distribution of carbon microspheres AC80 has a high degree of uniformity.

3.4. FTIR

The resulting FTIR spectroscopy diagrams of as-prepared carbon microspheres before and after the MB sorption are shown in Figure 4. These diagrams of the AC80 and AC40 samples are very similar, both before and after MB sorption. The changes after MB sorption are most pronounced in the fingerprint region in the range of 400 cm^{-1} to 1500 cm^{-1}, also very similar for both samples.

The foremost bands were found, assigning the broad O-H absorption band to the plan range from 3600 cm^{-1} to 3000 cm^{-1} and the C=O stretching absorption at 1700 cm^{-1}. The peak at about 3600 cm^{-1} is attributed to the phenolic functional group, so common to the carbon materials. The expansion of this OH peak towards 3000 cm^{-1} as well as the C=O stretching of the absorption at 1700 cm^{-1} indicate the very intense presence of a carboxyl group, another characteristic functional group for carbon. We assume that the presence of the overlapping of OH bands from phenolic and carboxyl groups can be noticed as a broad O-H absorption band with two peaks at 3600 cm^{-1} and 3000 cm^{-1}. The next characteristic functional group for carbon-based materials is the carbonyl group. The carbonyl C=O band is usually the most intense absorption band in a spectrum in the range 1820–1660 cm^{-1}.

The carbonyl band with a peak at about 1700 cm^{-1} can be seen in the spectra. The bands in the range of 1160–1370 and 1675–1790 cm^{-1} are attributed to the lactones functional groups [27,45,46]. Aliphatic hydrocarbon (-C-H) is found at approximately 2900 cm^{-1} and the band at 1620 cm^{-1} could be attributed to the C=C stretching of aromatic and furanic rings. These bands did not undergo significant changes even after sorption of MB, and this is valid for both AC80 and AC40. The characteristic bands due to C-O (acid, alcohol) stretching vibrations are observed in the range from 1300 cm^{-1} to 1000 cm^{-1}, while the band at 790 cm^{-1} is assigned to aromatic C-H out-of-plane bending vibrations [27]. These data reveal that these carbon microspheres contain an aromatic core and resident functionalities in their shell.

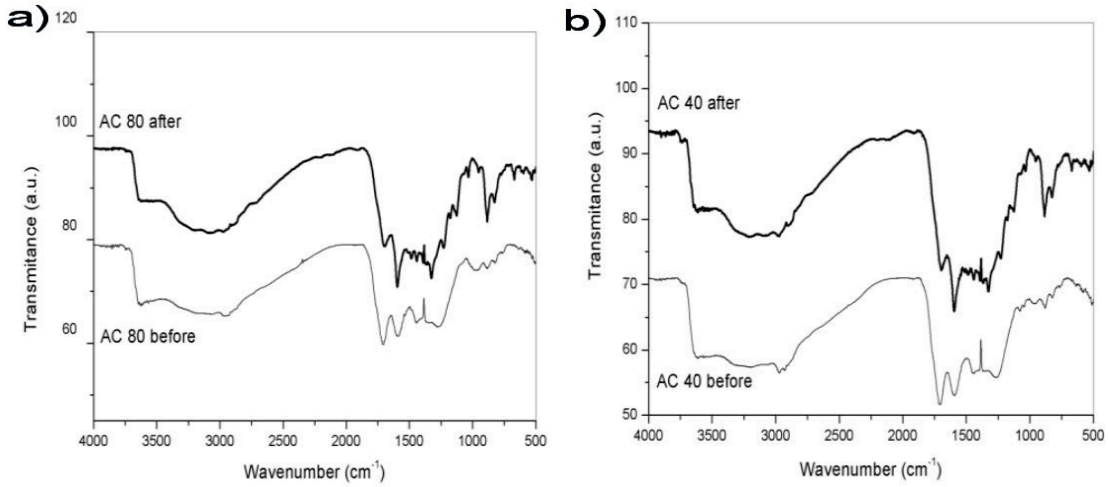

Figure 4. FTIR spectra of (**a**) AC80 and (**b**) AC40 carbon samples—before and after (thick line) sorption of MB.

Comparing the spectra recorded before and after the sorption, it is noticed that there is no significant difference in the position or shape of the bands observed in the spectra above 1700 cm^{-1}. However, the difference between the FTIR spectra recorded before and after MB sorption is noticed in the fingerprint region, pointing to the possible places of MB bonding to the surface of microspheres. Namely, the following changes can be observed on spectra upon sorption: (1) Presence of the stretching vibration of the carbonyl C=O bond before the sorption is confirmed by a strong band at 1705 cm^{-1}. After the sorption of MB, the band is shifted to 1697 cm^{-1} [47]. Then, the band observed at 1595 cm^{-1} can be attributed to the C=C starching vibrations of the aromatic ring [47]. It is not shifted after the sorption of MB, but the relative intensity of the peak increased after the MB sorption, so the peak intensity ratio of the C=O and C=C bands was changed. (2) The broad band noticed in the range 1300–1000 cm^{-1}, which originates from C-O stretching vibrations [45], disappeared after the MB sorption, and more bands appeared in the same range. (3) A slight shift of the band observed at 885 (from 879 to 885 cm^{-1}) and an increase in the band at 822 cm^{-1}, which can be attributed to the aromatic ring CH wagging [45] or out-of-plane bending [48] vibrations of carbon spheres, appeared in the spectrum after the MB sorption.

3.5. N_2 Adsorption/Desorption

The synthesized carbon microspheres AC80 and AC40 were also characterized by isotherms of N_2 adsorption/desorption at 77 K. The corresponding isotherms are presented in Figure 5. For both samples, similar isotherm profiles with microporous character were obtained.

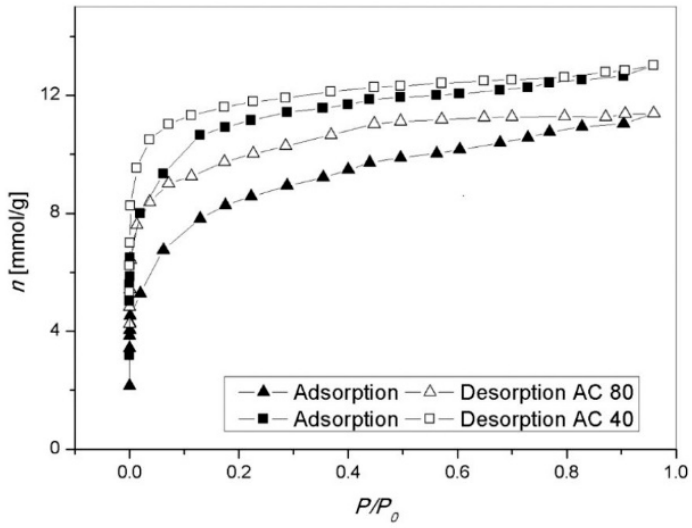

Figure 5. N_2 adsorption–desorption isotherms of carbon microspheres obtained by hydrothermal synthesis using H_3PO_4 with 40% and 80% concentration.

The presence of hysteresis indicates the presence of the mesopores. Also, low-pressure hysteresis could be attributed to irreversible uptake of adsorptive molecules in pores of about the same width as that of adsorbate molecules and/or swelling of nonrigid pore walls [38]. It is obvious from Figure 5 that the carbon microspheres prepared in solution with a lower concentration show better adsorption characteristics than the sample prepared with a higher concentration of activating acid. So, sample AC40 has a larger surface area (S_{BET}) and total pore volume (V_{tot}) than sample AC80; see Table 2. This was confirmed by further analysis shown below.

Table 2. N_2 adsorption/desorption characteristics of carbon microspheres obtained with different concentrations of H_3PO_4 solution.

Sample	S_{BET} (m^2/g)	V_{tot} (cm^3/g)	VDR (cm^3/g)	$V_{\alpha s}$ (cm^3/g)	E_0 (kJ/mol)	S_{mic} (m^2/g)	S_{ext} (m^2/g)	S_{tot} (m^2/g)
AC80	664	0.382	0.258	0.268	20.83	531	118	649
AC40	932	0.438	0.334	0.375	22.28	823	59	882

Results of specific surface areas calculated by the BET equation (S_{BET}) and other textural properties of the obtained samples are presented in Table 2. The values of S_{BET} for materials AC40 and AC80 are 932 m^2/g and 664 m^2/g, respectively. The dependence of the specific surface area on the applied concentration of phosphoric acid used as an activation agent is obvious. The values of S_{tot} for AC40 and AC80 are 882 m^2/g and 649 m^2/g, respectively, and these values are 2.3% and 5.7% lower, respectively, than those obtained by the BET method. The α_s method allows us to calculate the specific surface area of the microporous part of the sample (S_{mic}) as well as the part of the sample with meso- and macropores (S_{ext}). The external surface area (S_{ext}) is significantly lower than the microporous surface area (S_{mic}) for both samples, especially for sample AC40. These values are in agreement with the results obtained for total pores (V_{tot}) and micropore volumes. Values for VDR and E_0 obtained by applying D-R theory are also presented in Table 2. The values for E_0 of the carbon samples are about 20 and 22 kJ/mol, which could be attributed to the homogeneous structures of the obtained carbon microspheres. In fact, characteristic adsorption energy is related to pore width, and E_0 decreases as the micropore size distribution spreads to larger values. So, the sample with lower characteristic adsorption energy, in this case sample AC80, has larger pores. The fact that the micropore volume is near 30% higher for sample AC40 than for sample AC80 is confirmed by both calculation methods, α_s ($V_{\alpha s}$) and D-R (VDR). According to the HK method, the effective

pore size values (L) are between 0.35 and 1.5 nm. The values for mesopores (w) are below 4.5 nm.

3.6. Sorption of Methylene Blue

The effect of contact time on the MB removal by the tested samples for C_0 = 300 mg/dm^3, pH = 7, and at room temperature (25 °C) is shown in Figure 6. In the case of AC40, higher sorption capacities were attained for the same time relative to the sample AC80. Equilibrium in both cases was attained after 1320 min, although most of the sorption takes place in the first 150 min from the starting of the process. The superiority in terms of sorption performance of one sample over another is purely empirical. However, one could hypothesize that the textural properties of AC40, especially the more developed specific surface and pore structure, are responsible for the higher uptake of this sample.

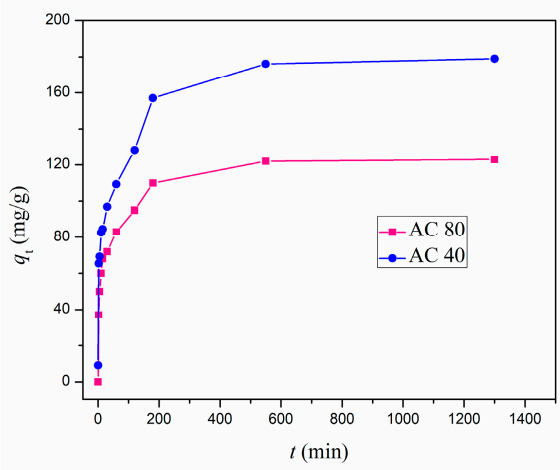

Figure 6. Effect of contact time on MB removal by obtained samples AC80 and AC40 (pH 7, C_0 300 mg/dm^3, T 25 °C).

The typical sorption isotherm depicting the dependence of sorption capacity from the residual MB concentration for equilibrium time conditions in the case of the sample AC40 is shown in Figure 7. The mass transfer driving force increases with the rising initial dye concentration and results in the boost in dye removal up to C_0 of 300 mg/dm^3 followed by a pronounced decrease after this point.

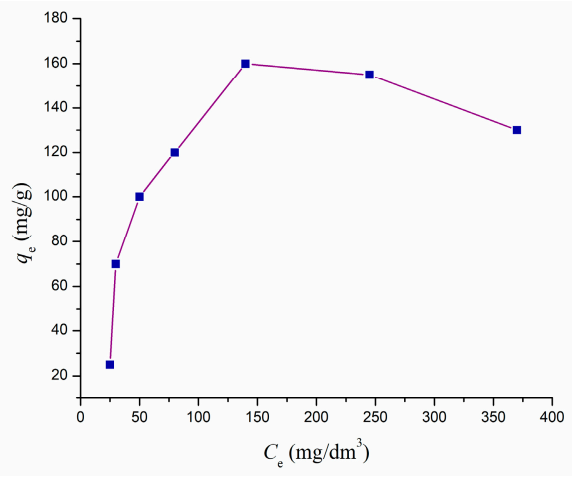

Figure 7. Effect of initial MB concentration on its removal related to sample AC40 (pH 7, 1320 min, T 25 °C).

In this study the maximum amount of MB sorption is reached at an initial concentration of C_0 300 mg/dm^3, reaching the final sorption capacity of 160 mg/g.

The effect of the initial solution pH on the sorption of MB onto the sample AC40 under the given experimental conditions is shown in Figure 8. As observed, the solution pH affects the amount of sorbed dye. The MB uptake was found to increase with increasing pH and it doubles with increasing pH from 5 to 12. The cationic dyes give positively charged ions when dissolved in water. Thus, in acidic mediums (lower pH), the positively charged surface of the sorbent tends to oppose the sorption of the cationic sorbent. As the pH of the dye solution is increased, the surface acquires a negative charge, resulting in an increased sorption of MB due to an increase in the electrostatic attraction between negatively charged sorbent and positively charged dye [49]. Due to the lowest MB removal extent at pH = 5, all the other experiments were carried out at pH 7 and 12. The sorption parameters were evaluated using the Langmuir isotherm model, which sums the formation of a monolayer on the sorbent surface and can be represented by the equation as follows:

$$\frac{C_e}{q_e} = \frac{1}{K_L q_m} + \frac{1}{q_m} C_e \quad (2)$$

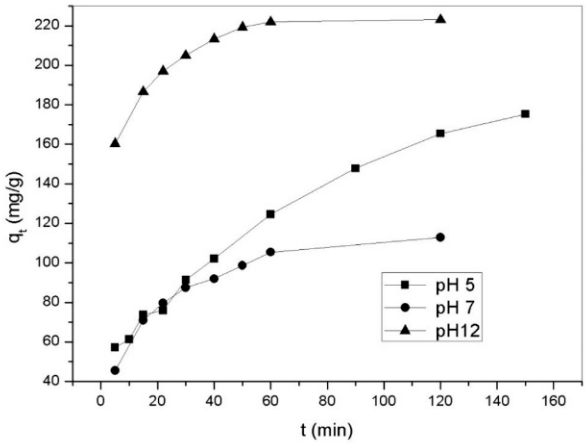

Figure 8. Effect of initial solution pH on the sorption of MB for the sample AC40 (C_0 300 mg/dm^3, T 25 °C).

In Equation (2), q_e and q_m are sorption capacities (mg/g) at equilibrium and at the monolayer, respectively. C_e is dye concentration at equilibrium in solution (mg/L). K_L is the Langmuir constant (L/mg) related to the affinity of binding sites and the free energy of sorption. A straight line was obtained when C_e/q_e was plotted against C_e; see Figure 9.

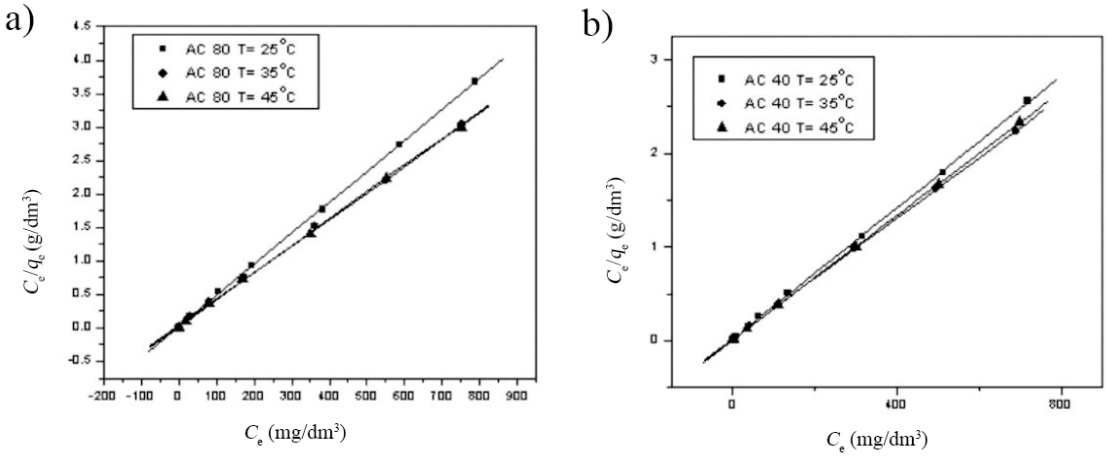

Figure 9. Effect of temperature on the MB sorption onto samples (**a**) AC80 and (**b**) AC40.

As can be seen from Figure 9, with increasing temperature, there is no increase in the sorption of dye. Room temperature proved to be the most efficient for MB sorption on the obtained samples of carbon microspheres.

Predicting batch sorption processes is essential for modeling sorption kinetics. In this study, the applicability of the pseudo-first-order and pseudo-second-order equations was tested for fitting the experimental data of MB sorption onto AC40 [50]. As per Lagergren's first-order model, a plot of log ($q_e - q_t$) versus t gives a straight line with a low linear regression coefficient (R^2), and it is therefore not presented here. The sorption data were then analyzed using the pseudo-second-order kinetic model [50]. The pseudo-second-order rate model is defined by the following Equation (3).

$$\frac{t}{q_t} = \frac{1}{k_2 q_e^2} + \frac{1}{q_e} t \quad (3)$$

where k_2 (min^{-1}) is the rate constant of the pseudo-second-order equation.

Figure 10 shows pseudo-second-order kinetic model fittings with experimental data for varying C_0 and pH. Plots between t/q_t versus t are straight lines with values of correlation coefficient R^2 in the range between 0.9902 and 0.9999; see Table 3. The values of k^2 and q_e were determined from the intercept and the slope of these plots. Kinetic parameters for the removal of MB by the obtained carbon microspheres are given in Table 3. The initial sorption rate, h (mg/g min) was used as a measure of sorption rate at the beginning of the sorption. The h can be determined by the following Equation (4):

$$h = k_2 q_e^2 \quad (4)$$

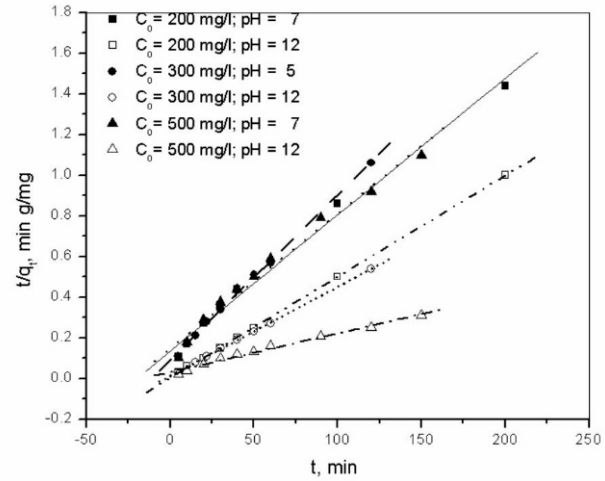

Figure 10. Pseudo-second-order kinetic model for MB sorption onto carbon microspheres AC40 at different C_0 and pH values.

Table 3. Pseudo-second-order kinetic parameters for MB sorption on carbon microspheres AC40.

C_0 (mg/dm ^{3})	200	200	300	300	500	500
pH	7	12	5	12	7	12
R^2	0.996	0.999	0.999	0.999	0.991	0.990
q_e (mg/g)	148.81	200.00	123.00	227.79	150.60	500.00
k_2 (g/mg min)	0.00034	0.00758	0.00073	0.00154	0.00030	0.00120
h (mg/g min)	7.53	303.20	11.04	79.91	6.80	300.00

The initial sorption rate h significantly increases at a higher pH.

According to the obtained results presented in Table 3, dye quantities sorbed onto the sorbent surface at equilibrium (q_e) significantly increase with pH increase. The sorption of MB in basic solution was described earlier [51].

4. Conclusions

The hydrothermal synthesis of carbon microspheres using fructose and phosphoric acid as an activating agent has demonstrated significant differences in the structural and sorption properties of the resulting materials depending on the concentration of H_3PO_4. The elemental analysis confirmed a high carbon content in both samples, while the XRPD patterns confirmed their amorphous structure. SEM analysis revealed that carbon microspheres synthesized with higher phosphoric acid concentration had smaller and more uniform diameters of particles compared to AC40. Most commonly, particles have diameters around 1.0 and 2.3 μm for AC80 and AC40, respectively. In addition, AC80 microspheres displayed a higher degree of uniformity. N_2 adsorption/desorption analysis demonstrated that the textural properties of the materials were highly influenced by the activation agent concentration. In the case of AC40, a larger surface area (932 m^2/g) and total pore volume (0.438 (cm^3/g)) was evidenced. While equilibrium required 1320 min to be reached for both sorbents, most sorption was completed within the initial 150 min. The sorption kinetics followed a pseudo-second-order model, with AC40 achieving faster and more efficient MB removal, especially at higher pH levels. It was shown that the sorption of dye does not improve with increasing temperature, making room temperature the most effective for MB sorption on both the carbon microsphere samples.

Overall, this study confirms that lower concentrations of H_3PO_4 in the synthesis process lead to carbon materials with superior sorption characteristics, making them a promising candidate for environmental applications such as dye removal from wastewater. Future research could further explore the optimization of synthesis parameters to enhance the removal properties.

Author Contributions: Conceptualization, S.S.K. and V.M.D.; methodology, S.S.K.; software, Đ.Č.; validation, Đ.Č. and R.T.V.; formal analysis, B.V.K., P.G., D.J., M.Z.M. and V.M.D.; investigation S.S.K.; writing—original draft preparation, B.V.K.; writing—review and editing, M.Z.M., B.V.K. and V.M.D.; visualization, R.T.V. and P.G. All authors have read and agreed to the published version of the manuscript.

Funding: This research was funded by the Ministry of Science, Technological Development and Innovation of the Republic of Serbia (Contract No. 451-03-68/2022-14/200017 and 451-03-66/2024-03/200124).

Data Availability Statement: The data presented in this study are available on request from the corresponding author. The data are not publicly available due to privacy.

Conflicts of Interest: Author Pavel Gurikov was employed by the company Aerogel-it GmbH. The remaining authors declare that the research was conducted in the absence of any commercial or financial relationships that could be construed as a potential conflict of interest. The funders had no role in the design of this study; in the collection, analyses, or interpretation of data; in the writing of the manuscript; or in the decision to publish the results.

References

1. Alnasrawi, F.A.M.; Kareem, S.L.; Mohammed Saleh, L.A. Adsorption of methylene blue from aqueous solution using different types of activated carbon. *J. Appl. Water Eng. Res.* **2022**, *11*, 370–380. [CrossRef]
2. Deepanraj, B.; Tirth, V.; Algahtani, A.; Elsehly, E.M. The performance of multi-walled carbon nanotubes-based filters with acid functionalization for enhanced methylene blue removal from water resources. *Alex. Eng. J.* **2024**, *88*, 310–316. [CrossRef]
3. Solanki, B.S.; Lim, H.; Yoon, S.J.; Ham, H.C.; Park, H.S.; Lee, H.E.; Lee, S.H. Recent advancement of non-noble metal catalysts for hydrogen production by NH_3 decomposition. *Renew. Sustain. Energy Rev.* **2025**, *207*, 114974. [CrossRef]
4. Wang, K.; Li, Z.; Gao, X.; Ma, Q.; Zhang, J.; Zhao, T.-S.; Tsubaki, N. Novel heterogeneous Fe-based catalysts for carbon dioxide hydrogenation to long chain α-olefins—A review. *Environ. Res.* **2024**, *242*, 117715. [CrossRef]

5. Kwarteng, F.A.; Abdel-Aty, A.A.R.; Mohamed, S.R.E.; Hassan, M.A.; Ohashi, H.; López-Salas, N.; Semida, W.M.; Khalil, A.S.G. Novel onion flower-derived biochar for high-performance sustainable supercapacitor applications. *Diam. Relat. Mater.* **2024**, *150*, 111703. [CrossRef]
6. Hayat, A.; Bashir, T.; Ahmed, A.M.; Ajmal, Z.; Alghamdi, M.M.; El-Zahhar, A.A.; Sohail, M.; Amin, M.A.; Al-Hadeethi, Y.; Ghasali, E.; et al. Novel 2D MBenes-synthesis, structure, properties with excellent performance in energy conversion and storage: A review. *Mater. Sci. Eng. R Rep.* **2024**, *159*, 100796. [CrossRef]
7. Ewii, U.E.; Onugwu, A.L.; Nwokpor, V.C.; Akpaso, I.; Ogbulie, T.E.; Aharanwa, B.; Chijioke, C.; Verla, N.; Iheme, C.; Ujowundu, C.; et al. Novel drug delivery systems: Insight into self-powered and nano-enabled drug delivery systems. *Nano Trans. Med.* **2024**, *3*, 100042. [CrossRef]
8. Luo, W.; Li, H.; Jin, M.; Liu, J.; Zhang, X.; Huang, G.; Zhou, T.; Lu, X. Organic frameworks (MOFs, COFs, and HOFs) based membrane materials for CO_2 gas-selective separation: A systematic review. *Sep. Purif. Technol.* **2025**, *357B*, 130195. [CrossRef]
9. Jareer, M.; Brijesh, K.; Safa, S.; Shahgaldi, S. The recent advancements in lithium-silicon alloy for next generation batteries: A review paper. *J. Alloys Compd.* **2025**, *1010*, 177124. [CrossRef]
10. Wang, Q.; Liang, X.Y.; Zhang, R.; Liu, C.J.; Liu, X.J.; Qiao, W.M.; Zhan, L.; Ling, L.C. Preparation of polystyrene-based activated carbon spheres and their adsorption of dibenzothiophene. *New Carbon Mater.* **2009**, *24*, 55–60. [CrossRef]
11. Derbyshire, F.; Jagtoyen, M.; MAndrews, R.; Rao, A.; Martin-Guillon, I.; Grulke, E.A. Carbon Materials in Environmental Applications. In *Chemistry and Physics of Carbon*; Radovick, L.R., Ed.; Marcel Dekker: New York, NY, USA, 2000; pp. 1–66.
12. Guo, P.; Gu, Y.; Lei, Z.; Cui, Y.; Zhao, X.S. Preparation of sucrose-based microporous carbons and their application as electrode materials for supercapacitors. *Micropor. Mesopor. Mater.* **2012**, *156*, 176–180. [CrossRef]
13. Wang, C.; Zhang, W.; Qiu, X.; Xu, C. Hydrothermal treatment of lignocellulosic biomass towards low-carbon development: Production of high-value-added bioproducts. *EnergyChem.* **2024**, *6*, 100133. [CrossRef]
14. Armandi, M.; Bonelli, B.; Geobaldo, F.; Garrone, E. Nanoporous carbon materials obtained by sucrose carbonization in the presence of KOH. Micropor. *Mesopor. Mater.* **2010**, *132*, 414–420. [CrossRef]
15. Singh, R.; Wang, L.; Cheng, J.; Sun, H.; Wu, C.; Huang, J. Synthesis of nitrogen-doped mesoporous carbon nanospheres using urea-phenol-formaldehyde resin for efficient CO_2 adsorption–desorption studies. *Carbon Capture Sci. Technol.* **2024**, *13*, 100302. [CrossRef]
16. Cui, X.J.; Antonietti, M.; Yu, S.H. Structural Effects of Iron Oxide Nanoparticles and Iron Ions on the Hydrothermal Carbonization of Starch and Rice Carbohydrates. *Small* **2006**, *2*, 756–759. [CrossRef]
17. Funke, A.; Ziegler, F. Hydrothermal carbonization of biomass: A summary and discussion of chemical mechanisms for process engineering. *Biofuels Bioprod. Biorefin.* **2010**, *4*, 160–177. [CrossRef]
18. Wan, W.; Zhao, W.; Wu, Y.; Dai, C.; Zhu, X.; Wang, Y.; Qin, J.; Chen, T. A highly efficient biomass based electrocatalyst for cathodic performance of lithium–oxygen batteries: Yeast derived hydrothermal carbon. *Electrochim. Acta* **2020**, *349*, 136411. [CrossRef]
19. Yuan, D.; Chen, J.; Zeng, J.; Tan, S. Preparation of monodisperse carbon nanospheres for electrochemical capacitors. *Electrochem. Commun.* **2008**, *10*, 1067–1070. [CrossRef]
20. Wang, Q.; Li, H.; Chen, L.; Huang, X. Monodispersed hard carbon spherules with uniform nanopores. *Carbon* **2001**, *39*, 2211–2214. [CrossRef]
21. Gong, Y.T.; Wang, H.Y.; Wei, Z.Z.; Xie, L.; Wang, Y. An efficient way to introduce hierarchical structure into biomass-based hydrothermal carbonaceous materials. *ACS Sustain. Chem. Eng.* **2014**, *2*, 2435–2441. [CrossRef]
22. Romero-Anaya, A.J.; Ouzzine, M.; Lillo-Ródenas, M.A.; Linares-Solano, A. Spherical carbons: Synthesis, characterization and activation processes. *Carbon* **2014**, *68*, 296–307. [CrossRef]
23. Wei, L.; Sevilla, M.; Fuertes, A.B.; Mokaya, R.; Yushin, G. Hydrothermal carbonization of abundant renewable natural organic chemicals for high-performance supercapacitor electrodes. *Adv. Energy Mater.* **2011**, *1*, 356–361. [CrossRef]
24. Yang, J.; Sudik, A.; Wolverton, C.; Siegel, D.J. High capacity hydrogenstorage materials: Attributes for automotive applications and techniques for materials discovery. *Chem. Soc. Rev.* **2010**, *39*, 656–675. [CrossRef]
25. Deshmukh, A.A.; Mhlanga, S.D.; Coville, N.J. Carbon spheres. *Mater. Sci. Eng. R* **2010**, *70*, 1–28. [CrossRef]
26. Sun, H.; Cao, L.; Lu, L. Magnetite/reduced graphene oxide nanocomposites: One step solvothermal synthesis and use as a novel platform for removal of dye pollutants. *Nano Res.* **2011**, *4*, 550–562. [CrossRef]
27. Ozcan, D.O.; Hendekci, M.C.; Ovez, B. Enhancing the adsorption capacity of organic and inorganic pollutants onto impregnated olive stone derived activated carbon. *Heliyon* **2024**, *10*, e032792. [CrossRef]
28. Sahu, A.; Poler, J.C. Removal and degradation of dyes from textile industry wastewater: Benchmarking recent advancements, toxicity assessment and cost analysis of treatment processes. *J. Environ. Chem. Eng.* **2024**, *12*, 113754. [CrossRef]
29. Munonde, T.S.; Madima, N.; Ratshiedana, R.; Nomngongo, P.N.; Mofokeng, L.E.; Dima, R.S. Synergistic adsorption-photocatalytic remediation of methylene blue dye from textile industry wastewater over NiFe LDH supported on tyre-ash derived activated carbon. *Appl. Surf. Sci.* **2025**, *679*, 161205. [CrossRef]
30. Yamjala, M.; Nainar, M.S.; Ramisetti, N.R. Methods for the analysis of azo dyes employed in food industry—A review. *Food Chem.* **2016**, *192*, 813–824. [CrossRef] [PubMed]
31. Murmu, G.; Panigrahi, T.H.; Saha, S. Recent advances in the development of polyoxometalates and their composites for the degradation of toxic chemical dyes. *Prog. Solid State Chem.* **2024**, *76*, 100489. [CrossRef]

32. Bhuyan, A.; Ahmaruzzaman, M. Recent advances in MOF-5-based photocatalysts for efficient degradation of toxic organic dyes in aqueous medium. *Next Sustain.* **2024**, *3*, 100016. [CrossRef]
33. Xie, F.; Phillips, J.; Silva, I.F.; Palma, M.C.; Menendez, J.A. Microcalorimetric study of acid sites on ammonia- and acid-pretreated activated carbon. *Carbon* **2000**, *38*, 691–700. [CrossRef]
34. Hu, C.C.; Wang, C.C. Effects of electrolytes and electrochemical pretreatments on the capacitive characteristics of activated carbon fabrics for supercapacitors. *J. Power Sources* **2004**, *125*, 299. [CrossRef]
35. Sivaranjanee, R.; Kumar, P.S.; Rangasamy, G. Hydrothermally produced activated carbon spheres from discarded maize cobs for efficient removal of rose bengal dye from water environment. *Desal. Water Treat.* **2024**, *317*, 100123. [CrossRef]
36. Kamath, A.A.; Nayak, N.G.; Sagar, R.; Kamath, A.K. Hibiscus leaf petiole derived activated carbon as a potential sorbent for basic green 4 and reactive yellow 15 dye exclusion from aqueous solution. *Inorg. Chem. Commun.* **2024**, *168*, 112903. [CrossRef]
37. Cherdoud, F.; Khelifi, S.; Reffas, A. Activated carbons developed from Algerian agro-waste of palm trunk fiber: Characterization and adsorptive capacity for azo dyes removal. *Desal. Water Treat.* **2023**, *311*, 118–134. [CrossRef]
38. Gregg, S.J.; Sing, K.S.W. *Adsorption, Surface Area and Porosity*, 2nd ed.; Academic Press: London, UK, 1982; pp. 411–432.
39. Rouquerol, F.; Rouquerol, J.; Sing, K. *Adsorption by Powders and Porous Solids*; Academic Press: London, UK, 1999; pp. 105–110.
40. Hutson, N.D.; Yang, R.T. Theoretical basis for the Dubinin-Radushkevitch (D-R) adsorption isotherm equation. *Adsorption* **1997**, *3*, 189–195. [CrossRef]
41. Horvath, G.; Kawazoe, K. Method for the calculation of effective pore size distribution in molecular sieve carbon. *J. Chem. Eng. Jpn.* **1983**, *16*, 470–475. [CrossRef]
42. Barrett, E.P.; Joyner, L.G.; Halenda, P.P. The determination of pore volume and area distributions in porous substances. I. Computations from nitrogen isotherms. *J. Am. Chem. Soc.* **1951**, *73*, 373–380. [CrossRef]
43. Kaneko, K.; Yamguchi, K.; Ishii, C.; Ozeki, S.; Hagi-Wara, S.; Suzuki, T. Size evaluation of graphitic crystallites in activated carbon fibers from diamagnetic susceptibility measurements. *Chem. Phys. Lett.* **1991**, *176*, 75–78. [CrossRef]
44. Kaneko, K.; Ishii, C.; Kanoh, H.; Hanzawa, Y.; Setoyama, N.; Suzuki, T. Characterization of porous carbons with high resolution αs-analysis and low temperature magnetic susceptibility. *Adv. Colloid Interface Sci.* **1998**, *76–77*, 295–320. [CrossRef]
45. Larkin, P. *Infrared and Raman Spectroscopy: Principles and Spectral Interpretation*; Elsevier: Amsterdam, The Netherlands, 2011; pp. 158–205. [CrossRef]
46. Tucureanu, V.; Matei, A.; Avram, A.M. FTIR Spectroscopy for Carbon Family Study. *Crit. Rev. Anal. Chem.* **2016**, *46*, 502–520. [CrossRef] [PubMed]
47. Fathy, M.; El-Sayed, M.; Ramzi, M.; AbdelRaheem, O.H. Adsorption separation of condensate oil from produced water using ACTF prepared of oil palm leaves by batch and fixed bed techniques. *Egypt. J. Pet.* **2018**, *27*, 319–326. [CrossRef]
48. Kumar, M.; Srivastava, M.; Yadav, R.A. Vibrational studies of benzene, pyridine, pyridine-N-oxide and their cations. *Spectrochim. Acta A* **2013**, *111*, 242–251. [CrossRef] [PubMed]
49. Pathania, D.; Sharma, S.; Singh, P. Removal of methylene blue by adsorption onto activated carbon developed from Ficus carica bast. *Arab. J. Chem.* **2017**, *10*, S1445–S1451. [CrossRef]
50. Ho, Y.S.; McKay, G. Sorption of dye from aqueous solution by peat. *Chem. Eng. J.* **1998**, *70*, 115–124. [CrossRef]
51. Boumediene, M.; Benaïssa, H.; George, B.; Molina, S.; Merlin, A. Effects of pH and ionic strength on methylene blue removal from synthetic aqueous solutions by sorption onto orange peel and desorption study. *J. Mater. Environ. Sci.* **2018**, *9*, 1700–1711. [CrossRef]